Research Square

Preprints are preliminary reports that have not undergone peer review.
They should not be considered conclusive, used to inform clinical practice,
or referenced by the media as validated information.

Effect of temperature and composition on density, viscosity, surface tension and refractive index for 2-HEAA + CPAc, 2-HEAA + HEAPe, and CPAc + HEAPe binary mixtures at atmospheric pressure

Francisco M. T. Pereira Filho
Universidade Federal do Ceará
Vitor J. Policarpo
Universidade Federal do Ceará
Lorena M. Alexandre e Silva
Empresa Brasileira de Pesquisa Agropecuária
Kirley M. Canuto
Empresa Brasileira de Pesquisa Agropecuária
Filipe X. Feitosa
Universidade Federal do Ceará
Hosiberto B. Sant'Ana
hbs@ufc.br
Universidade Federal do Ceará

Research Article

Keywords: Protic ionic liquids, Thermophysical properties, Binary mixtures, Excess molar volume, Eyring–NRTL, Atmospheric pressure

Posted Date: October 28th, 2026

DOI: https://doi.org/10.21203/rs.3.rs-11381541/v1

License: This work is licensed under a Creative Commons Attribution 4.0 International License.
Read Full License

Additional Declarations: No competing interests reported.

Effect of temperature and composition on density, viscosity, surface tension and refractive index for 2-HEAA + CPAc, 2-HEAA + HEAPe, and CPAc + HEAPe binary mixtures at atmospheric pressure

*Francisco M. T. Pereira Filho[a], Vitor J. Policarpo[a], Lorena M. Alexandre e Silva[b], Kirley M. Canuto[b], Filipe X. Feitosa[a], Hosiberto B. de Sant'Ana[a],**

[a] Grupo de Pesquisa em Termofluidodinâmica Aplicada, Department of Chemical Engineering, Universidade Federal do Ceará, Fortaleza, CE, Brazil

[b] Empresa Brasileira de Pesquisa Agropecuária (Embrapa), Fortaleza, CE, Brazil

*Corresponding author

Hosiberto B. de Sant'Ana · hbs@ufc.br

Abstract

Density and dynamic viscosity were measured for binary mixtures of 2-hydroxyethanaminium acetate (2-HEAA), 2-hydroxyethanaminium pentanoate (HEAPe), and caprolactam acetate (CPAc) from 293.15 to 373.15 K at 101.3 kPa. Surface tension was measured from 293.15 to 343.15 K, and refractive index from 293.15 to 353.15 K. The three systems were 2-HEAA + CPAc, 2-HEAA + HEAPe, and CPAc + HEAPe. Excess molar volume and deviations in viscosity, surface tension, and refractive index were calculated and correlated with the Redlich–Kister equation. Excess molar volumes were predominantly negative, consistent with contraction relative to ideal mixing. Viscosity deviations changed sign in the first two systems and were negative throughout the measured interior compositions of CPAc + HEAPe. Refractive-index deviations were mostly positive; for CPAc + HEAPe they reached 0.017, indicating a positive excess molar refraction of about 3% that is attributed to the accommodation of flexible pentanoate chains and hydrogen-bond donors around the rigid lactam rings. Surface-tension deviations were predominantly negative for the two 2-HEAA systems, with positive values only in the dilute region of 2-HEAA + CPAc, and positive at all 54 interior points of CPAc + HEAPe, reaching +11.92 $mN \cdot m^{-1}$. An Eyring–NRTL correlation reproduced the viscosities of 2-HEAA + HEAPe with an average absolute relative deviation of 0.92%, whereas the corresponding deviations were 12.76% and 6.23% for 2-HEAA + CPAc and CPAc + HEAPe. These data provide thermophysical properties and mixing information for the three ionic-liquid pairs at atmospheric pressure.

Keywords: Protic ionic liquids · Thermophysical properties · Binary mixtures · Excess molar volume · Eyring–NRTL · Atmospheric pressure

1 Introduction

Ionic liquids (IL) are a class of compounds formed by organic cations and anions of different sizes, which are liquids at room temperature. These solvents have a melting point below 373.15 K and have recently been studied from academic and industrial viewpoints as green process precursors because of their unique physicochemical properties [1–3]. Moreover, they can exhibit nanoheterogeneity in the liquid state depending on carbon chain length; this arises from the coexistence of polar and nonpolar parts at the nanoscale, driven by interactions among ions [4–6].

Another essential feature is the ability of imidazole-based ionic liquids to reduce surface tension in binary mixtures, principally with water, making them excellent extraction solvents [7, 8]. In addition to being less harmful to the environment [9], they are less toxic and have a lower vapor pressure than other organic solvents [10]. As a classification, they are classified into (i) protic ionic liquids (PILs) and (ii) aprotic ionic liquids (APILs) [11].

Protic ionic liquids (PILs) form via a Brønsted acid-based stoichiometric reaction using amino group cations as a base, which simplifies the process and reduces synthesis costs, making it possible to reuse and even recycle the compounds [12–14]. PILs have been used as catalysts for the tert-butylation of phenol and esterification of alkenes with acetic acid [15], as solvents for carbon dioxide absorption [16, 17], as polymer electrolyte membranes [18], and as biosensors [19], among other applications. One of the most critical factors distinguishing it from APILs is the presence of at least one proton capable of promoting hydrogen bonds, interacting strongly with polar solvents [20].

Caprolactam-based ionic liquids (CPILs) [21] are less toxic than imidazole-based ionic liquids [22]. In addition, carboxylate-based ionic liquids can dissolve cellulose and lignocellulose during the biofuel production process [23].

However, for the industrial development and application of these PILs, a still-scarce database of thermophysical and thermodynamic properties that can describe the behavior of ionic liquids themselves or their mixtures with other solvents [24–28] is necessary. Given such needs, it is essential to determine specific properties such as viscosity, density, and surface tension for industrial and scientific issues.

Viscosity plays a fundamental role in dissolving substances such as biomass composites. However, high viscosity slows enzyme-catalyzed hydrolysis, which does not occur in CPIL because of its low viscosity [23]. On the other hand, density data give

access to the excess molar volume, which shows whether the components pack more or less efficiently on mixing than in the pure liquids [13]. Density and viscosity are mainly affected by the cation's chemical properties, while miscibility and thermal stability are directly related to the anion; depending on the objective, it is possible to choose the most suitable ion combination [24–26, 29–31]. Surface tension is also important, as it can affect the rate of vapor absorption at the liquid-vapor interface and indicate that specific ILs act as surfactants and may form micelles in aqueous solution or reverse micelles in nonpolar solvents [27, 28]. These properties can be modified by changing the IL cation or anion, so it is possible to develop ILs with ideal characteristics for a given process [32].

Therefore, this work aims to study two protic ionic liquids, ammonium-based (2-hydroxyethanaminium acetate [2-HEAA] and 2-hydroxyethanaminium pentanoate [HEAPe]), and caprolactam-based ionic liquid (caprolactam acetate [CPAc]), through experimental measurements of density (ρ), dynamic viscosity (η), surface tension (σ) and refractive index of three binary mixtures of ionic liquids (2-HEAA + CPAc, 2-HEAA + HEAPe, CPAc + HEAPe) over the temperature range T = (293.15 to 373.15) K for density and dynamic viscosity, (293.15 to 343.15) K for surface tension, and (293.15 to 353.15) K for refractive index for whole composition ranges and atmospheric pressure. After obtaining these properties, other derived thermodynamic properties were calculated, such as dynamic viscosity deviation ($\Delta\eta$), surface tension deviation ($\Delta\sigma$), excess molar volume (V^E), and refractive index deviation, to better understand the intermolecular interactions among pure ionic liquids and their mixtures; ATR-FTIR spectra of the mixtures were also recorded at 298.15 K.

2 Materials and Methods

2.1 Ionic Liquid Characterization

The ionic liquids used in this work were synthesized in our Research Group, as previously described in literature [33, 34]. Table 1 presents all chemical compounds used to synthesize the ILs studied in this work. Nuclear Magnetic Resonance (^{1}H NMR) determined the ILs' molecular structure. The water content of the samples was determined by Karl Fischer titration; Fourier-transform infrared spectroscopy (FTIR) was used to

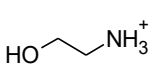
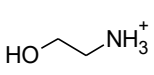
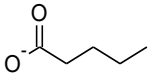
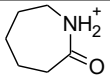
assess molecular structure. For additional information, see Online Resource 1. Table 2 provides IL specifications: structure, name, abbreviation, and CAS number.

Table 1 Sample description of the chemicals used in this work

Chemical name	CAS RN	M / g·mol⁻¹	Source	Initial purity[a]	Prep.	Purity[b]	Tests
acetic acid	64-19-7	60.05	Sigma-Aldrich	≥0.997	none	0.997	–
pentanoic acid	109-52-4	102.13	Sigma-Aldrich	≥0.990	none	0.980	–
ε-caprolactam	105-60-2	113.16	Sigma-Aldrich	≥0.990	none	0.990	–
2-aminoethan-1-ol (ethanolamine)	141-43-5	61.08	Dinâmica	≥0.990	none	0.990	–
2-hydroxyethan-1-aminium acetate (2-HEAA)	54300-24-2	121.14	synthesis[c]	–	vacuum drying[d]	0.975	^{1}H NMR, FTIR, KF
2-hydroxyethan-1-aminium pentanoate (HEAPe)	–	163.22	synthesis[c]	–	vacuum drying[d]	0.988	^{1}H NMR, FTIR, KF
caprolactam acetate (CPAc)	–	173.21	synthesis[c]	–	vacuum drying[d]	0.995	^{1}H NMR, FTIR, KF

[a] Initial reagent purity is the mass fraction reported by the supplier. [b] Purity is the nonwater mass fraction determined by Karl Fischer titration; [c] Synthesized in our laboratory by the stoichiometric Brønsted acid–base reaction between the amine and the carboxylic acid (Section 2.1). [d] Synthesized liquids were dried under vacuum at 333.15 K and 20 kPa for 48 h.

Table 2 Ionic liquids Structure, Name, and Abbreviation.

Cation	Anion	Name	Abbreviation
		2-hydroxyethanaminium acetate	2-HEAA
		2-hydroxyethanaminium pentanoate	HEAPe
		caprolactam acetate	CPAc

Binary mixtures of ionic liquids were prepared in Falcon tubes (50 mL) by adding the previously specified quantities of the substances to achieve a molar fraction range of 0.05 to 0.95, using an electronic analytical balance with a precision of ± 0.0001 g.

The resulting mixtures were vortexed to ensure complete homogenization. They were then stored in a vacuum oven for 24 hours before measurements were taken. We took care

not to expose them to ambient light to prevent degradation and ensure the components were not contaminated, especially by water.

2.2 Density and Viscosity Measurements

The pure substances' density and dynamic viscosity measurements, and those of their respective mixtures (2-HEAA + CPAc, 2-HEAA + HEAPe, CPAc + HEAPe), were performed on an Anton-Paar SVM 3000 viscodensimeter. Measurements were made at T = (293.15 to 373.15) K and at atmospheric pressure (101.3 kPa). Our group also reported the densities of pure 2-HEAA and HEAPe at 0.1 MPa in a previous high-pressure study [35], on a different temperature grid (298.15, 313.15, 333.15, 353.15 and 373.15 K). The two data sets are therefore independent determinations of the same isobar, and Section 2.7 compares them. Table 4 lists the values measured in the present work. For 2-HEAA + HEAPe, the mole fractions reported for the viscosity series (Table 5) differ from those of the density series (Table 4); where the two properties are combined (Eyring–NRTL, Section 2.6), the molar volume at the viscosity compositions was obtained from the Redlich–Kister correlation of V^E.

The standard uncertainty of temperature was taken as u(T) = 0.05 K, the value adopted in our group's most recent density study [36]and is used as a conservative estimate; the resulting temperature terms are listed in Table S12. The standard uncertainty of each reported mole fraction was obtained from its three-decimal resolution, assuming a rectangular interval of ±0.0005: $u(x_1) = 0.0005/\sqrt{3} = 0.00029$; the weighing contribution (±0.0001 g on samples of about 15 g) is negligible. The combined standard uncertainty of each measured property was evaluated following the GUM as reported in supplementary material. The uncertainty for density and viscosity, respectively, are $u(\rho) = 0.0014$ g·cm^{-3} and $u(\eta) = 0.0147\eta$.

2.3 Surface Tension Measurements

Surface tension measurements were performed on a Krüss tensiometer with a resolution of 0.01 mN·m^{-1} at temperatures T = (293.15 to 343.15) K, using du Noüy ring method to obtain the results. The technique uses a ring, generally made of platinum-iridium, to apply a specific force on the fluid surface. This technique has reasonable accuracy, especially for more viscous liquids measured with the Harkins–Jordan correction factor [37, 38].

A Julabo F32 bath controlled the sample temperature, monitored by a thermocouple. The standard temperature uncertainty u(T) = 0.05 K was adopted from our group's most recent high-pressure density study [36]. The ring was cleaned by flaming, tared, immersed, and evaluated with the instrument correction factor.

Four ring readings were averaged at each nominal temperature; their pooled standard deviation is 0.055 mN·m^{-11}. Combined with the instrument resolution (0.01 mN·m^{-1}, rectangular distribution) and the temperature contribution (≤ 0.015 mN·m^{-1}), $u_c(\sigma)$ = 0.25 mN·m^{-1}.

2.4 Refractive Index Measurements

Refractive index (nD) was measured using a Anton Parr Abbemat 550 refractometer at T = (293.15 to 353.15) K and atmospheric pressure. No replicate refractive-index readings were available, so u(nD) was evaluated from the refractometer accuracy (±0.0002, rectangular distribution), the reporting resolution (0.0001) and the temperature contribution (≤ 0.00002), giving u_c(nD) = 0.00012. Ultrapure water (18.2 MΩ·cm) was used for instrument calibration.

2.5 Derived Properties

From density, dynamic viscosity, surface tension, and refractive index experimental data, it is possible to calculate, respectively, excess molar volume (V^E / cm^3·mol^{-1}), dynamic viscosity deviation ($\Delta\eta$ / mPa·s), surface tension deviation ($\Delta\sigma$ / mN·m^{-1}) and refractive index deviation (Δn_D) of the mixtures using equations 1 to 4.

$$V^E = \sum_{i=1}^{N} x_i M_i (\rho^{-1} - \rho_i^{-1}) \quad (1)$$

$$\Delta\eta = \eta - \sum_{i=1}^{N} x_i \eta_i \quad (2)$$

$$\Delta\sigma = \sigma - \sum_{i=1}^{N} x_i \sigma_i \quad (3)$$

$$\Delta n_D = n_D - \sum_{i=1}^{N} x_i n_{D_i} \quad (4)$$

where ρ, η, σ and n_D denote the density, dynamic viscosity, surface tension, and refractive index of the mixture, respectively; N is the number of components, x_i, ρ_i, η_i, σ_i, n_{D_i}, and M_i denote molar fraction, density, dynamic viscosity, surface tension, refractive index, and molar mass of the pure compounds.

Excess and deviation properties were correlated by using the Redlich-Kister equation:

$$y = x_i(1 - x_i)\sum_{j=0}^{k} A_j(1 - 2x_i)^j \quad (5)$$

where y is V^E, $\Delta\eta$, $\Delta\sigma$ or Δn_D; A_j are the adjusted parameters, and k is the degree of polynomial expansion obtained through a polynomial adjustment using the least-squares fitting procedure. The corresponding standard deviations were given by:

$$s(y) = \sqrt{\frac{\sum(y_{exp} - y_{cal})^2}{(n - p)}} \quad (6)$$

where y_{exp} is the experimental excess properties, and y_{cal} is the calculated excess properties, n is the number of experimental points, and p is the number of parameters used in the adjustment procedure.

2.6 Eyring–NRTL Viscosity Model

According to Eyring's absolute reaction rate theory, viscous flow is approached as an activation process. Due to the close analogy between excess flow activation energy and excess free energy of mixing, the Eyring-NRTL [40] equation can be written as follows:

$$\ln(\eta V) = x_1 \ln(\eta_1 V_1) + x_2 \ln(\eta_2 V_2) + x_1 x_2 \left[\frac{\tau_{21} G_{21}}{x_1 + x_2 G_{21}} + \frac{\tau_{12} G_{12}}{x_2 + x_1 G_{12}}\right], \quad G_{ij} = \exp(-\alpha \tau_{ij}) \qquad (7)$$

$$\tau_{ij} = \frac{\Delta g_{ij}}{RT} \qquad (8)$$

Here η and V are mixture viscosity and molar volume; x_i, η_i and V_i refer to the pure components. We fixed α = 0.25. The binary interaction energies were taken as linearly temperature dependent:

$$\Delta g_{ij}(T) = \Delta g_{ij}(T_{\text{ref}}) + (T - T_{\text{ref}}) \Delta g_{ij}^{1}, \quad T_{\text{ref}} = 333.15 \text{ K} \qquad (9)$$

The four coefficients were obtained by bounded nonlinear least squares of the log-viscosity residuals in Equation 10. Molar volumes were calculated from the measured densities. For 2-HEAA + HEAPe, whose viscosity and density series were reported at different mole fractions, the molar volume at each viscosity composition was obtained as the ideal volume plus the Redlich–Kister correlation of V^E at the same temperature (Table S6), so that the volumes used in the model are consistent with the reported excess volumes.

$$\text{O. F.} = \sum_{i=1}^{n} \left[\frac{\ln(\eta^i) - \ln(\eta_{exp}^i)}{\ln(\eta_{exp}^i)}\right]^2 \qquad (10)$$

2.7 Comparison with Literature

Figure 1 compares the available density, viscosity and surface-tension measurements of the pure substances with reported values. Relative differences were calculated from the literature average and the present experimental data:

$$\text{err\%} = 100 \cdot \frac{|y_{lit} - y_{exp}|}{y_{lit}} \qquad (11)$$

where y_{lit} is the literature average and y_{exp} is the experimental data. The values available in the literature: 2-HEAA (density [14, 41, 42], viscosity [41, 42]), HEAPe (density [43, 44], viscosity [43, 44], surface tension [43]), CPAc (density [34, 45], viscosity [34, 45]). Relative differences reach about 1.1 % for density, 17 % for viscosity and 6 % for surface tension (Fig. 1), well above the uncertainties of the present measurements. Surface tensions of 2-HEAA and CPAc could not be compared for lack of literature data. Refractive indices are not compared in Fig. 1, because literature values were found only for 2-HEAA [14] and not for HEAPe or CPAc.

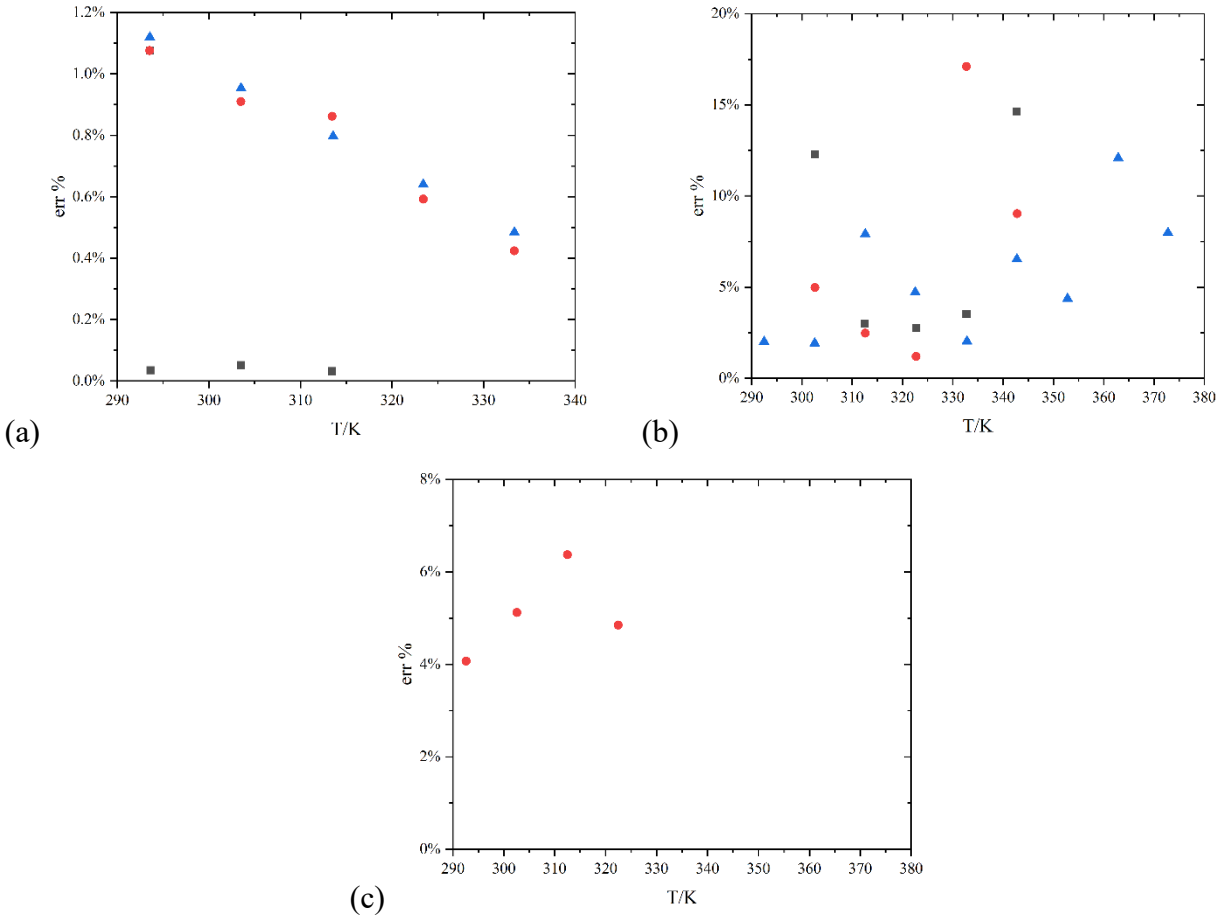


Fig. 1 Relative differences from available literature data: (a) density, 2-HEAA (▲), HEAPe (●), CPAc (▪); (b) viscosity, same symbols; (c) surface tension, HEAPe (●)

The observed inconsistencies, particularly in the viscosity data, likely stem from non-uniform experimental conditions. Variations in synthesis and purification procedures,

measurement techniques, and the limited amount of published data may all contribute to these discrepancies. Dias, Sosa, and Costa [41] reported similar problems and also emphasized that these properties are highly sensitive to impurities. This only strengthens the need for additional experimental data.

We also compared the pure-component densities measured in this work with the 0.1 MPa isobar reported by our group for 2-HEAA and HEAPe in a previous high-pressure study [35]. Because the two studies were carried out on different temperature grids, the comparison constitutes an independent check rather than a repetition of the same measurement: the average absolute relative deviation is 0.09 % for 2-HEAA and 0.12 % for HEAPe, with a maximum single-point deviation of 0.24 %. The root-mean-square difference of this comparison, 0.0014 $g \cdot cm^{-3}$, was adopted as the reproducibility of the density measurements (Section 2.2).

3 Results and Discussion

3.1 Structural Characterization of the Ionic Liquids

The spectra of the isolated products show prominent FTIR transmittance minima near 1524 and 1398 cm^{-1} for both 2-HEAA and HEAPe, and near 1621 cm^{-1} for CPAc (Fig. 2). The paired bands for 2-HEAA and HEAPe are consistent with carboxylate stretching, whereas the CPAc feature lies in the lactam carbonyl region. These observations, together with the ^{1}H NMR shifts in Table 3, support the proposed product structures [34, 46].

The product spectra differ from those of the acid and base precursors in band position and intensity. Features near 900–940 cm^{-1} also change after synthesis. Because vibrational bands overlap in these regions, such intensity changes do not by themselves quantify acid deprotonation or hydrogen-bond strength [47, 48].

A change or apparent loss of a feature near 800–865 cm^{-1} does not establish the disappearance of N–H bonds or independently prove ion-pair formation. The spectral interpretation therefore rests on the combined FTIR and ^{1}H NMR observations rather than on a single band [49].

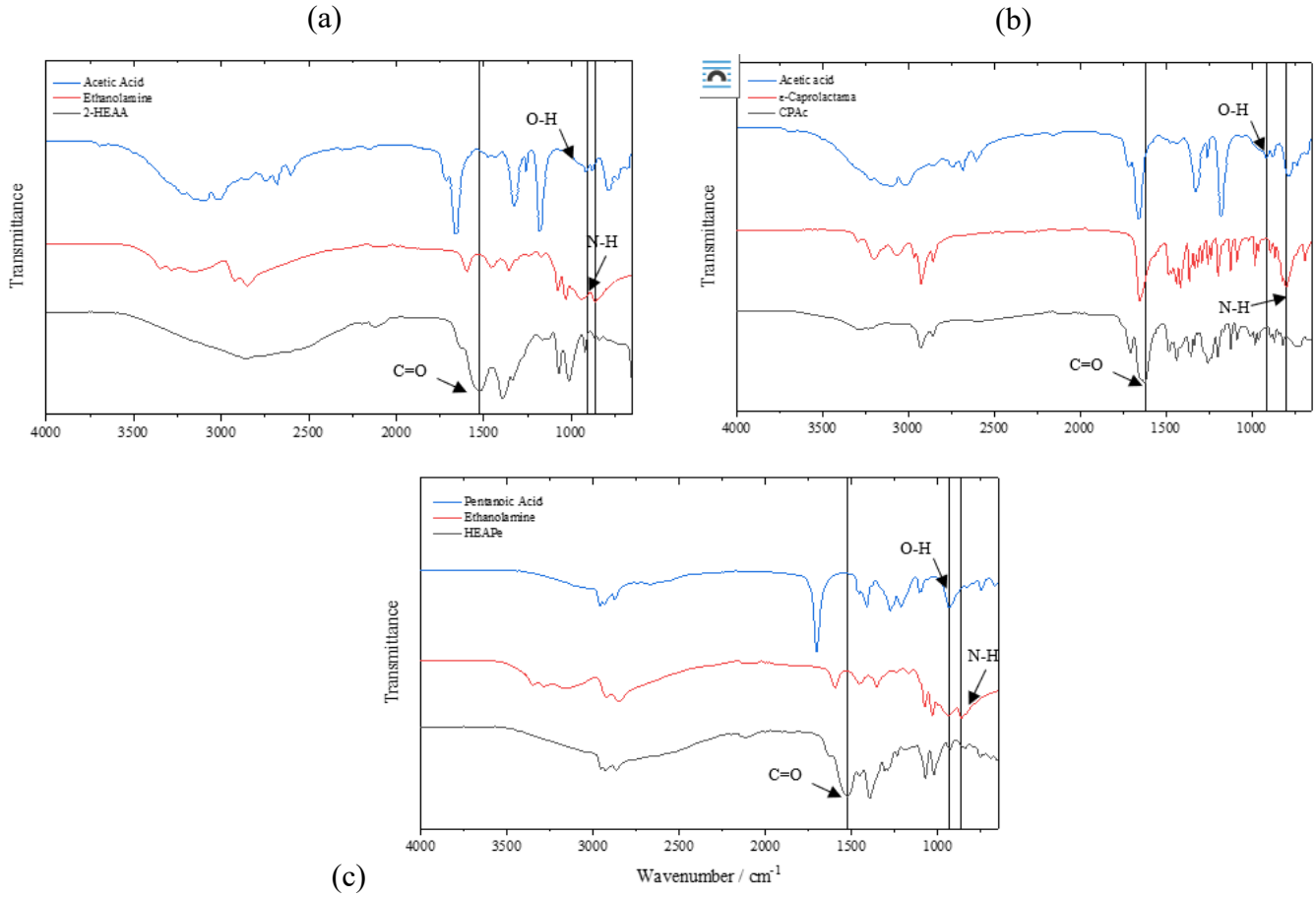


Fig. 2 FTIR transmittance spectra of the reactants and isolated products: (a) acetic acid, ethanolamine, and 2-HEAA; (b) acetic acid, ε-caprolactam, and CPAc; (c) pentanoic acid, ethanolamine, and HEAPe. The arrows near 1524 cm^{-1} in panels (a) and (c) identify the product carboxylate band region

Table 3 compares the ^{1}H NMR chemical shifts of the precursor mixtures and isolated products. The exchangeable N–H signal changes from 6.25 to 5.83 ppm for 2-HEAA and from 5.10 to 4.54 ppm for HEAPe; the CPAc ^{1}H signal changes from 7.41 to 7.19 ppm. These differences indicate changes in local proton environments after synthesis, but do not quantify proton transfer, ion pairing, or hydrogen-bond strength.

The ^{1}H NMR spectra of the ionic liquids are shown in Figs. S1, S2, and S3 (Online Resource 1).

Table 3 ^{1}H NMR chemical shifts of the precursor mixtures (SM) and isolated products. *NH denotes an exchangeable-proton signal and does not assign a fixed NH_2 or NH_3^+ stoichiometry from chemical shift alone

H	2-HEAA		HEAPe		CPAc	
	δ^1H(ppm) SM	δ^1H(ppm) IL	δ^1H(ppm) SM	δ^1H(ppm) IL	δ^1H(ppm) SM	δ^1H(ppm) IL
1	2.75	2.75	2.65	2.72	7.41	7.19
2	3.51	3.71	3.43	3.49		
3	1.67	1.68	1.90	1.95	2.45	2.45
4	-	-	1.37	1.39	1.67	1.67
5	-	-	1.20	1.21	2.05	2.04
6	-	-	0.80	0.81	3.19	3.19
NH*	6.25	5.83	5.10	4.54		

3.2 Experimental Thermophysical Properties

The experimental data of density (ρ), dynamic viscosity (η), surface tension (σ), and refractive index (n_D) of the binary mixtures (2-HEAA + CPAc, 2-HEAA + HEAPe, CPAc + HEAPe) in temperatures T = (293.15 to 373.15) K for density and dynamic viscosity, (293.15 to 343.15) K for surface tension, and (293.15 to 353.15) K for refractive index, at atmospheric pressure (101.3 kPa), are listed in Tables 4-7.

Table 4 Density data (ρ) for studied IL mixtures at T = (293.15 to 373.15) K and atmospheric pressure (101.3 kPa). *

x_1	ρ / g·cm^{-3}								
	T/ K								
	293.15	303.15	313.15	323.15	333.15	343.15	353.15	363.15	373.15
2-HEAA (1) + CPAc (2)									
1.000	1.1536	1.1481	1.1424	1.1368	1.1311	1.1256	1.1199	1.1141	1.1082
0.857	1.1427	1.1369	1.1310	1.1252	1.1195	1.1137	1.1079	1.1017	1.0956
0.730	1.1309	1.1248	1.1184	1.1125	1.1065	1.1006	1.0945	1.0881	1.0819
0.615	1.1189	1.1124	1.1060	1.0998	1.0936	1.0872	1.0810	1.0747	1.0685
0.505	1.1073	1.1006	1.0941	1.0874	1.0809	1.0744	1.0678	1.0611	1.0543
0.423	1.0941	1.0872	1.0804	1.0735	1.0667	1.0599	1.0531	1.0463	1.0390
0.312	1.0847	1.0777	1.0707	1.0635	1.0564	1.0494	1.0420	1.0348	1.0277
0.225	1.0754	1.0673	1.0598	1.0525	1.0451	1.0375	1.0300	1.0225	1.0152
0.147	1.0623	1.0546	1.0470	1.0392	1.0315	1.0237	1.0159	1.0075	0.9998
0.071	1.060	1.052	1.044	1.036	1.028	1.020	1.012	1.004	0.9963
0.000	1.059	1.051	1.044	1.035	1.028	1.019	1.011	1.003	0.9955
2-HEAA (1) + HEAPe (2)									
1.000	1.1536	1.1481	1.1424	1.1368	1.1311	1.1256	1.1199	1.1141	1.1082
0.841	1.1399	1.1341	1.1283	1.1226	1.1169	1.1111	1.1054	1.0994	1.0932
0.705	1.1284	1.1226	1.1167	1.1108	1.1050	1.0992	1.0932	1.0871	1.0809
0.577	1.1143	1.1084	1.1024	1.0964	1.0904	1.0845	1.0784	1.0724	1.0659
0.467	1.1031	1.0973	1.0913	1.0852	1.0792	1.0732	1.0671	1.0609	1.0544
0.373	1.0938	1.0878	1.0817	1.0757	1.0697	1.0636	1.0576	1.0516	1.0456
0.285	1.0831	1.0771	1.0709	1.0647	1.0585	1.0523	1.0461	1.0396	1.0332

0.202	1.0733	1.0672	1.0610	1.0547	1.0485	1.0424	1.0361	1.0296	1.0230
0.126	1.0631	1.0569	1.0506	1.0442	1.0379	1.0317	1.0252	1.0187	1.0121
0.000	1.0480	1.0418	1.0355	1.0291	1.0227	1.0169	1.0103	1.0037	0.9971
CPAc (1) + HEAPe (2)									
1.000	1.059	1.051	1.044	1.035	1.028	1.019	1.011	1.003	0.9955
0.949	1.0601	1.0522	1.0443	1.0364	1.0285	1.0205	1.0125	1.0045	0.9970
0.882	1.0627	1.0553	1.0475	1.0399	1.0322	1.0245	1.0167	1.0090	1.0013
0.775	1.0610	1.0535	1.0461	1.0386	1.0312	1.0236	1.0162	1.0086	1.0011
0.671	1.0582	1.0511	1.0438	1.0364	1.0291	1.0220	1.0145	1.0072	1.0000
0.578	1.0559	1.0488	1.0417	1.0346	1.0276	1.0205	1.0133	1.0061	0.9994
0.467	1.0543	1.0475	1.0408	1.0339	1.0271	1.0202	1.0132	1.0061	0.9993
0.320	1.0526	1.0459	1.0394	1.0330	1.0265	1.0199	1.0133	1.0065	0.9997
0.179	1.0503	1.0438	1.0374	1.0311	1.0248	1.0183	1.0118	1.0050	0.9985
0.113	1.0497	1.0433	1.0369	1.0307	1.0244	1.0179	1.0114	1.0046	0.9981
0.000	1.0480	1.0418	1.0355	1.0291	1.0227	1.0169	1.0103	1.0037	0.9971

* Standard uncertainties: $u(x_1) = 0.00029$, $u(T) = 0.05$ K, and $u_c(\rho) = 0.0014$ g·cm^{-3}.

Table 5 Viscosity (η) for studied IL mixtures at T = (293.15 to 373.15) K and atmospheric pressure (101.3 kPa). *

	η /mPa·s								
	T / K								
x_1	293.15	303.15	313.15	323.15	333.15	343.15	353.15	363.15	373.15
2-HEAA (1) + CPAc (2)									
1.000	2404	1045	505.3	267.4	152.6	92.16	59.12	39.67	27.56
0.857	2381	1033	500.7	265.0	151.5	92.24	59.18	39.63	27.49
0.730	1476	656.6	327.2	178.0	104.6	65.41	43.03	29.46	20.86
0.615	964.3	441.6	225.6	126.2	76.08	48.73	32.80	21.71	15.75
0.505	536.4	254.8	135.7	78.78	49.06	32.35	22.38	16.08	11.89
0.423	344.4	170.4	93.40	55.70	35.58	24.03	16.99	12.50	9.565
0.312	181.3	93.81	53.59	33.21	21.96	15.30	11.12	8.350	6.444
0.225	99.71	54.12	32.33	20.82	14.23	10.21	7.610	5.853	4.617
0.147	49.98	28.95	18.27	12.34	8.786	6.529	5.024	3.979	3.263
0.071	34.39	20.42	13.16	9.060	6.559	4.947	3.857	3.093	2.555
0.000	38.41	22.23	14.09	9.587	6.883	5.156	3.997	3.190	2.617
2-HEAA (1) + HEAPe (2)									
1.000	2404	1045	505.3	267.4	152.6	92.16	59.12	39.67	27.56
0.874	2542	1114	558.8	297.3	170.1	103.5	66.26	44.27	30.62
0.798	2559	1150	570.0	306.5	176.5	107.7	69.06	46.22	31.71
0.715	2548	1158	579.5	313.6	181.3	110.8	71.07	47.41	32.69
0.627	2532	1162	584.6	317.7	184.2	112.8	72.23	48.04	32.98
0.533	2448	1138	579.4	317.7	185.3	113.9	73.23	48.93	33.82
0.423	2409	1132	579.2	320.7	187.4	115.2	73.98	49.21	33.63
0.295	2368	1129	584.8	324.5	190.3	117.8	75.76	50.54	34.81
0.159	2283	1095	569.6	317.0	186.5	115.2	73.96	49.03	33.53
0.000	2401	1162	608.6	340.0	200.5	122.6	78.65	52.17	35.51
CPAc (1) + HEAPe (2)									
1.000	38.41	22.23	14.09	9.587	6.883	5.156	3.997	3.190	2.617
0.949	47.81	27.92	17.47	11.72	8.307	6.152	4.718	3.734	3.035
0.882	77.76	42.23	25.10	16.11	11.02	7.937	5.946	4.607	3.669
0.775	93.49	51.06	30.57	19.70	13.46	9.641	7.179	5.522	4.367
0.671	147.1	78.94	46.35	29.26	19.61	13.80	10.10	7.467	5.954
0.578	196.2	104.8	61.06	38.18	25.35	17.64	12.77	9.560	7.352
0.467	308.4	162.4	93.17	57.25	37.29	25.48	18.10	13.28	9.996
0.320	562.0	291.0	163.4	98.12	62.34	41.49	28.69	20.38	14.94
0.179	861.5	441.6	244.7	144.5	89.98	58.85	39.53	27.51	19.64
0.113	1103	557.2	304.6	177.4	108.9	69.87	46.53	31.97	22.54

0.000	2401	1162	608.6	340.0	200.5	122.6	78.65	52.17	35.51

* Standard uncertainties: u(x_1) = 0.00029, u(T) = 0.05 K, and $u_c(\eta)$ = 0.015η (Online Resource 1).

Table 6 Surface Tension (σ) for studied IL mixtures at T = (293.15 to 343.15) K and atmospheric pressure (101.3 kPa). *

x_1	σ / mN·m^{-1}					
	T / K					
	293.15	303.15	313.15	323.15	333.15	343.15
2-HEAA (1) + CPAc (2)						
1.000	52.98	52.15	50.80	49.33	48.10	47.00
0.857	45.60	45.03	44.10	43.00	42.00	41.00
0.730	42.65	41.78	40.68	39.58	38.53	37.40
0.615	41.40	40.30	39.40	37.85	37.05	35.45
0.505	40.61	39.61	38.50	37.20	36.30	35.00
0.423	40.05	39.05	38.10	36.80	35.80	34.60
0.312	39.80	38.80	37.90	36.50	35.50	34.50
0.225	39.70	38.70	37.70	36.20	35.20	34.20
0.147	39.65	38.65	37.65	36.50	35.30	34.50
0.071	39.15	38.18	37.13	35.20	34.08	33.53
0.000	35.80	35.30	34.30	33.43	32.53	31.50
2-HEAA (1) + HEAPe (2)						
1.000	52.98	52.15	50.80	49.33	48.10	47.00
0.841	43.90	43.35	42.30	41.35	40.23	39.40
0.705	39.08	38.33	37.58	36.33	34.95	33.30
0.577	37.70	36.93	36.03	35.20	34.10	32.80
0.467	36.93	36.03	35.20	34.25	33.10	31.70
0.373	36.08	35.03	34.18	33.28	32.30	31.28
0.285	34.90	34.10	33.10	32.00	31.33	30.13
0.202	34.44	33.75	32.75	31.65	30.53	29.40
0.126	33.50	32.60	31.60	30.55	29.45	28.15
0.000	33.18	32.30	31.45	30.58	29.50	28.50
CPAc (1) + HEAPe (2)						
1.000	35.80	35.30	34.30	33.43	32.53	31.50
0.949	40.79	40.27	39.35	38.86	37.39	36.67
0.882	44.83	44.28	43.30	42.61	41.10	40.42
0.775	47.13	46.53	45.37	43.97	42.96	42.01
0.671	46.72	46.05	44.82	43.19	42.46	41.29
0.578	45.70	44.97	43.81	42.47	41.62	40.42
0.467	44.89	44.07	43.10	42.26	41.08	40.01
0.320	45.00	44.11	43.28	42.27	41.13	40.20
0.179	44.35	43.44	42.47	40.16	39.88	38.80
0.113	42.34	41.43	40.39	37.67	37.71	36.52
0.000	33.18	32.30	31.45	30.58	29.50	28.50

* Standard uncertainties: u(x_1) = 0.00029, u(T) = 0.05 K, and $u_c(\sigma)$ = 0.25 mN·m^{-1}.

Table 7 Refractive index data (n_D) for studied IL mixtures at T = (293.15 to 353.15) K and atmospheric pressure (101.3 kPa). *

x_1	n_D						
	***T*/ K**						
	293.15	303.15	313.15	323.15	333.15	343.15	353.15
2-HEAA (1) + CPAc (2)							
1.000	1.4705	1.4682	1.4659	1.4635	1.4611	1.4586	1.4561
0.814	1.4688	1.4663	1.4639	1.4614	1.4589	1.4564	1.4539

0.652	1.4667	1.4642	1.4617	1.4591	1.4564	1.4536	1.4509
0.532	1.4652	1.4624	1.4596	1.4568	1.4540	1.4512	1.4483
0.421	1.4634	1.4604	1.4575	1.4545	1.4515	1.4485	1.4454
0.330	1.4614	1.4583	1.4552	1.4521	1.4490	1.4459	1.4430
0.245	1.4598	1.4565	1.4533	1.4500	1.4467	1.4434	1.4401
0.181	1.4573	1.4539	1.4506	1.4472	1.4438	1.4405	1.4375
0.109	1.4555	1.4520	1.4485	1.4449	1.4413	1.4377	1.4341
0.053	1.4523	1.4486	1.4449	1.4412	1.4374	1.4337	1.4306
0.000	1.4496	1.4459	1.4421	1.4382	1.4343	1.4304	1.4265
2-HEAA (1) + HEAPe (2)							
1.000	1.4705	1.4682	1.4659	1.4635	1.4611	1.4586	1.4561
0.832	1.4698	1.4674	1.4650	1.4626	1.4601	1.4576	1.4550
0.687	1.4694	1.4669	1.4645	1.4620	1.4594	1.4568	1.4541
0.562	1.4691	1.4666	1.4640	1.4614	1.4587	1.4560	1.4533
0.352	1.4684	1.4658	1.4632	1.4605	1.4578	1.4549	1.4521
0.121	1.4666	1.4639	1.4611	1.4582	1.4553	1.4523	1.4493
0.059	1.4663	1.4635	1.4606	1.4576	1.4547	1.4516	1.4486
0.000	1.4662	1.4633	1.4604	1.4574	1.4544	1.4513	1.4482
CPAc (1) + HEAPe (2)							
1.000	1.4496	1.4459	1.4421	1.4382	1.4343	1.4304	1.4265
0.887	1.4673	1.4638	1.4602	1.4567	1.4532	1.4499	1.4464
0.776	1.4681	1.4647	1.4613	1.4578	1.4543	1.4507	1.4470
0.664	1.4678	1.4645	1.4611	1.4578	1.4544	1.4510	1.4477
0.562	1.4675	1.4643	1.4611	1.4578	1.4545	1.4511	1.4477
0.468	1.4668	1.4636	1.4604	1.4573	1.4541	1.4510	1.4478
0.369	1.4667	1.4636	1.4605	1.4573	1.4541	1.4509	1.4477
0.276	1.4662	1.4631	1.4601	1.4571	1.4540	1.4508	1.4476
0.198	1.4658	1.4628	1.4598	1.4567	1.4537	1.4506	1.4475
0.091	1.4653	1.4624	1.4595	1.4565	1.4534	1.4502	1.4470
0.000	1.4662	1.4633	1.4604	1.4574	1.4544	1.4513	1.4482

* Standard uncertainties: $u(x_1) = 0.00029$, $u(T) = 0.05$ K, and $u_c(nD) = 0.00012$.

Density and dynamic viscosity decrease with increasing temperature in every tabulated series. Surface tension decreases with increasing temperature in every tabulated series except CPAc + HEAPe at $x_1 = 0.113$, where the values at 323.15 and 333.15 K (37.67 and 37.71 $mN \cdot m^{-1}$) agree within their expanded uncertainty.

At 293.15 K, the pure-component densities follow 2-HEAA > CPAc > HEAPe. CPAc is much less viscous than the other two pure liquids, whereas HEAPe is more viscous than 2-HEAA from 303.15 K upward. Density and viscosity therefore do not follow a common ranking across these compounds; the measured trends alone cannot isolate effects of chain length, cation geometry, or hydrogen bonding.

The density ordering of 2-HEAA and HEAPe is consistent with the independent high-pressure study discussed in Section 2.7. This agreement supports the density trend, but does not establish which intermolecular contribution controls mixing or viscous flow [35].

3.3 Excess Molar Volume

Figure 3 shows predominantly negative excess molar volumes. For 2-HEAA + CPAc, positive values occur at $x_1 = 0.071$ and 0.147, reaching +1.10 $cm^3 \cdot mol^{-1}$ at $x_1 = 0.147$ and 373.15 K; the minimum is −2.08 $cm^3 \cdot mol^{-1}$ at $x_1 = 0.615$ and 373.15 K. All interior values for 2-HEAA + HEAPe are negative, with a minimum of −2.32 $cm^3 \cdot mol^{-1}$ at $x_1 = 0.373$ and 373.15 K. All 81 interior values for CPAc + HEAPe are negative; at x_1(CPAc) = 0.179 and 363.15 K, $V^E = -0.23$ $cm^3 \cdot mol^{-1}$. Negative V^E denotes contraction relative to the ideal-volume reference and does not, by itself, identify a unique molecular mechanism.

The ATR-FTIR spectra of the mixtures were measured at 298.15 K (Fig. 4). In 2-HEAA + CPAc, features near 1068 and 1621 cm^{-1} shift toward 1084 and 1625 cm^{-1}, and a feature near 1255 cm^{-1} moves toward 1277 cm^{-1}. These observations show composition-dependent spectral changes at the measured temperature; they cannot establish the cause of the V^E trend over the full temperature interval.

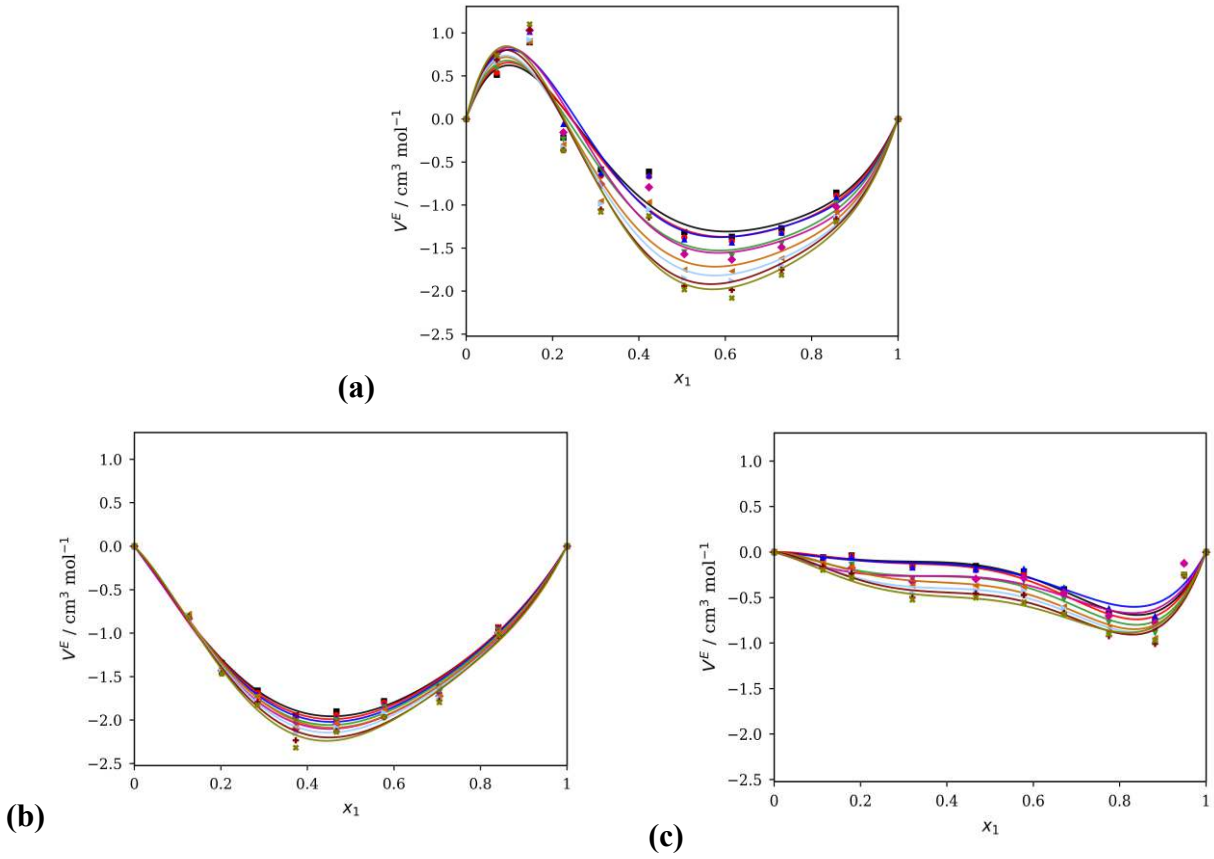


Fig. 3 Influence of temperature on the excess molar volume of binary mixture: (a) 2-HEAA (1) + CPAc (2); (b) 2-HEAA (1) + HEAPe (2); (c) CPAc (1) + HEAPe (2). Temperatures: (■) 293.15 K, (●) 303.15 K, (▲) 313.15 K, (▼) 323.15 K, (♦) 333.15 K,

(◄) 343.15 K, (►) 353.15 K, ( ) 363.15 K, and ( ) 373.15 K. All lines were obtained by polynomial adjustment of Redlich−Kister equation

The band near 1703 cm^{-1} changes mainly in intensity across the composition series, without a resolved shift in its reported position. Changes in intensity can reflect changing component proportions and local environments, whereas a change in band frequency requires a demonstrable change in peak position. The spectra therefore do not establish a direct connection between this band and the signs of V^E or $\Delta\sigma$.

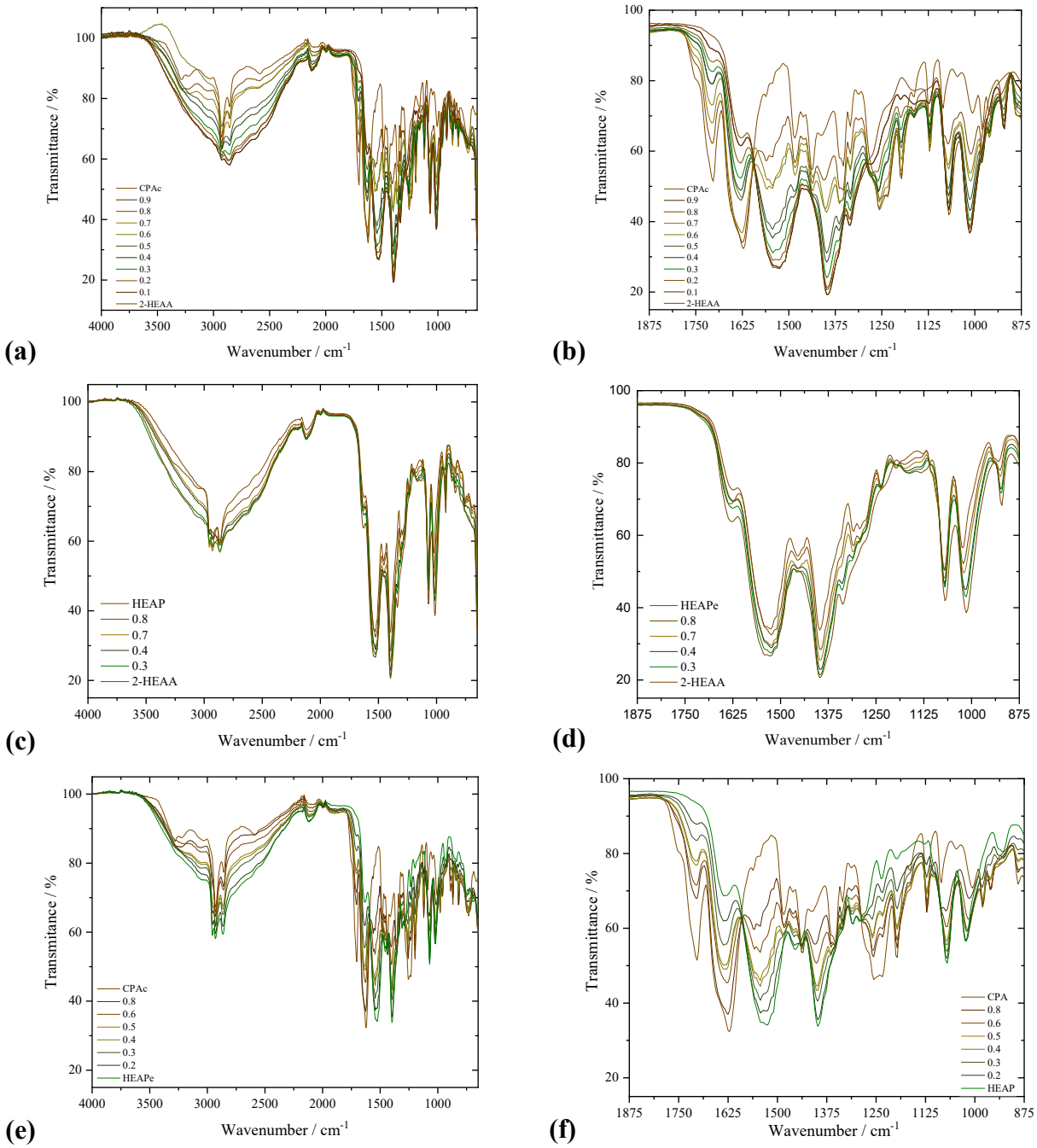


Fig. 4 ATR-FTIR for binary systems obtained at 298.15 K and atmospheric pressure: **(a)** CPAc + 2-HEAA; **(b)** CPAc + 2-HEAA. **(c)** HEAPe + 2-HEAA; **(d)** HEAPe + 2-HEAA. **(e)** CPAc + HEAPe; **(f)** CPAc + HEAPe.

For 2-HEAA + HEAPe (Figs. 4c and 4d), features near 1068 and 1307 cm^{-1} move toward 1084 and 1336 cm^{-1}, and the intensity near 1524 cm^{-1} varies with composition. The pronounced negative V^E values indicate nonideal volume contraction. The spectral changes are consistent with altered local environments but cannot separate packing, hydrogen-bonding and ionic contributions to that contraction [50].

For CPAc + HEAPe (Figs. 4e and 4f), features near 1069 and 1526 cm^{-1} move toward 1085 and 1542 cm^{-1}. The intensities of bands near 1704 and 1255 cm^{-1} decrease as the CPAc fraction decreases. Because these intensity changes accompany a change in component proportion, they cannot by themselves quantify a change in bond strength or explain the observed V^E trend [47].

3.4 Dynamic Viscosity Deviation

Figure 5 shows that the sign and magnitude of $\Delta\eta$ depend on composition. For 2-HEAA + CPAc, the minimum is −696 mPa·s at x_1 = 0.505 and 293.15 K, while positive deviations occur in the 2-HEAA-rich region. For 2-HEAA + HEAPe, the maximum is +156 mPa·s at x_1 = 0.798 and 293.15 K; the deviation changes sign across the composition range. CPAc + HEAPe has negative deviations at every interior point, reaching −1117 mPa·s at x_1(CPAc) = 0.179 and 293.15 K. The magnitude of the negative minimum decreases with temperature in each system, but the composition of the minimum does not shift in a common direction. $\Delta\eta$ exceeds its expanded uncertainty at 78 of 81, 53 of 72 and 81 of 81 interior points for the three systems, respectively; the unresolved values lie close to the sign changes.

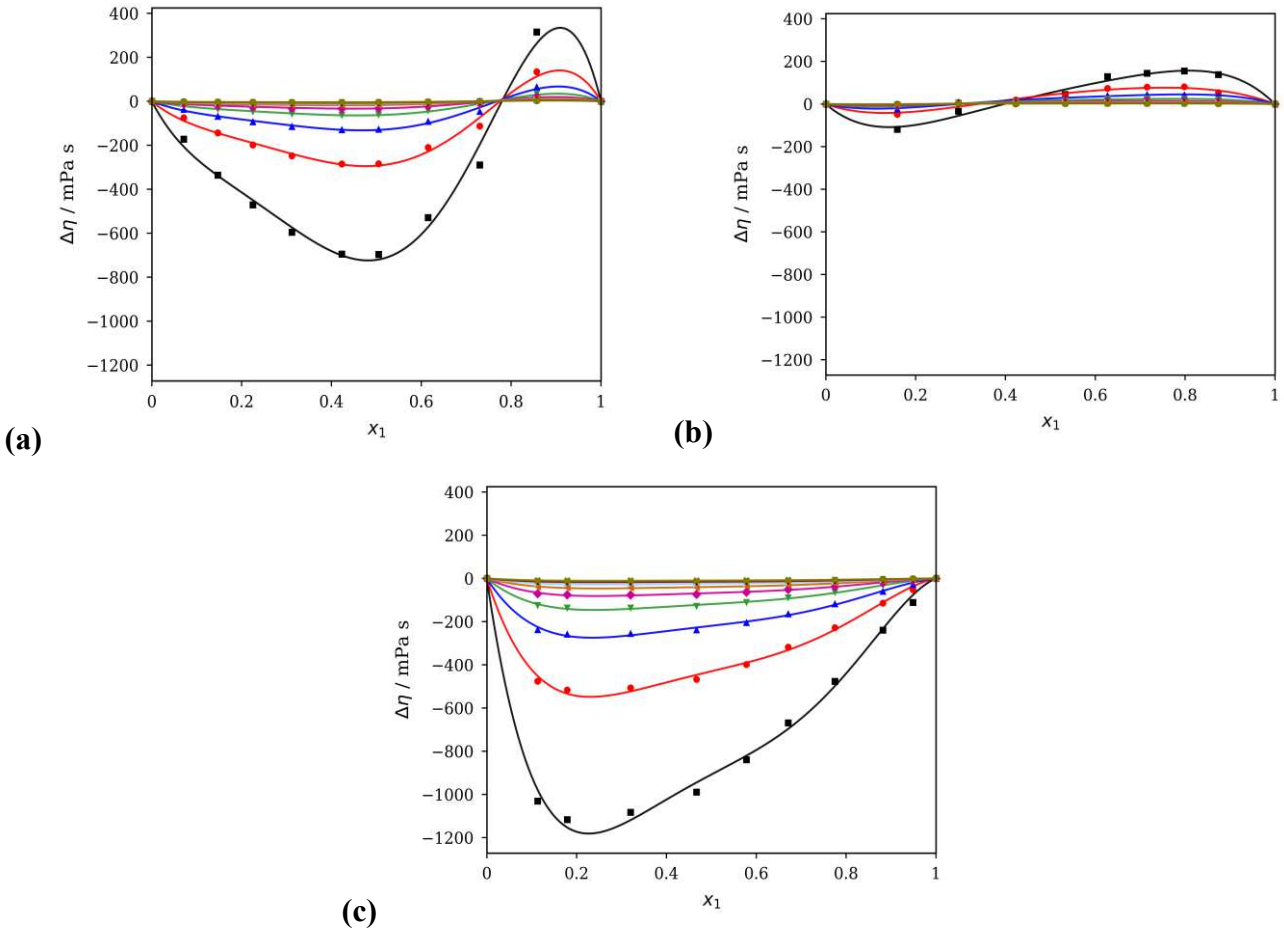


Fig. 5 Influence of temperature on the viscosity deviation of binary mixture: (a) 2-HEAA (1) + CPAc (2); (b) 2-HEAA (1) + HEAPe (2); (c) CPAc (1) + HEAPe (2). Temperatures: (■) 293.15 K, (●) 303.15 K, (▲) 313.15 K, (▼) 323.15 K, (♦) 333.15 K, (◄) 343.15 K, (►) 353.15 K, ( ) 363.15 K, and ( ) 373.15 K. All lines were obtained by polynomial adjustment of Redlich−Kister equation.

All measured mixture viscosities decrease as temperature increases. At a fixed temperature, Δη compares the mixture viscosity with a mole-fraction-weighted average of pure-component viscosities; a negative value does not imply that the mixture is less viscous than both pure components. The deviations demonstrate nonlinearity with composition, but their signs alone do not identify the interactions responsible for viscous flow [51].

3.5 Eyring–NRTL Viscosity Model

Figure 6 compares measured viscosities with the Eyring–NRTL correlation fitted over the measured temperature and composition range. The residuals by composition and

temperature are shown in Fig. S19. The model describes 2-HEAA + HEAPe substantially more closely than the other two systems and is used here as a correlation within the investigated range.

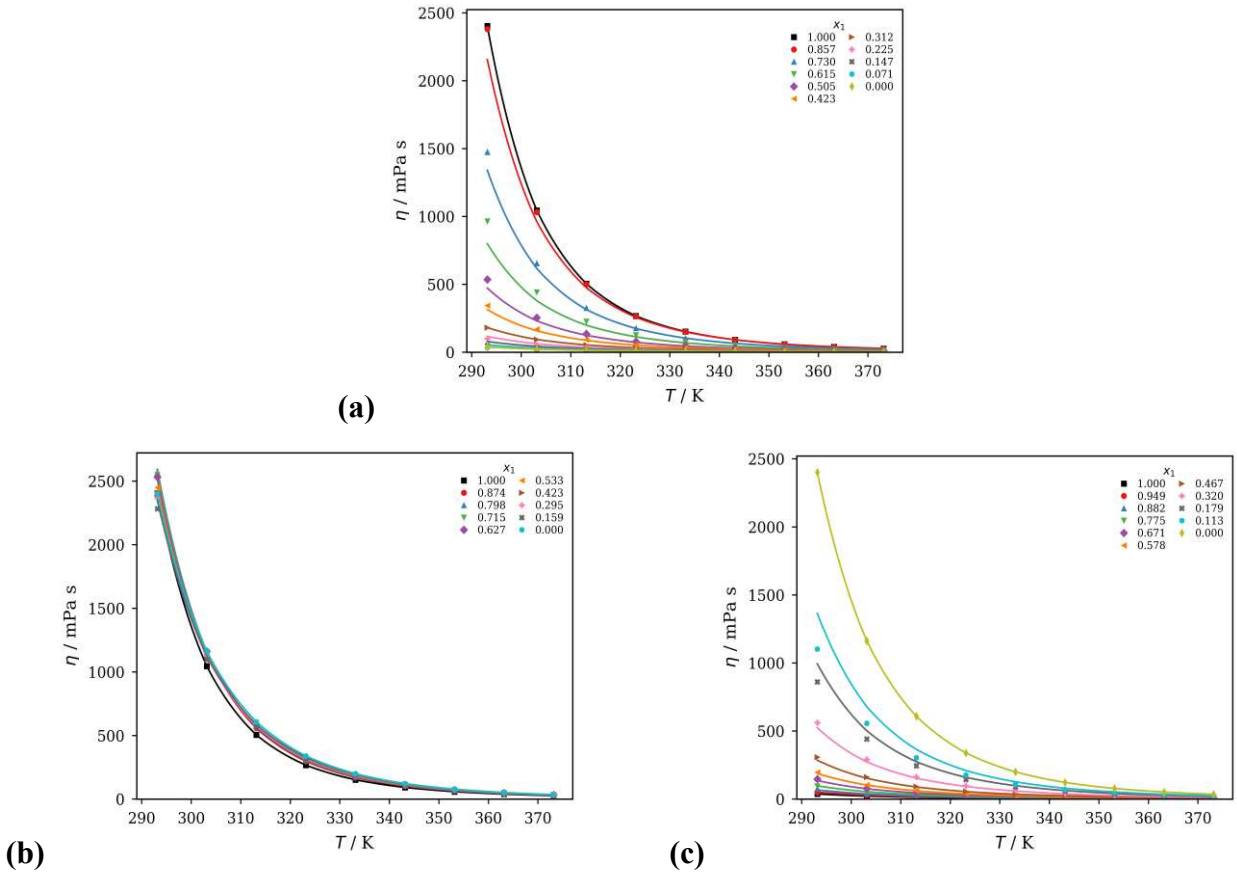


Fig. 6 Measured dynamic viscosities (symbols) and Eyring–NRTL calculated values (lines) for (a) 2-HEAA (1) + CPAc (2), (b) 2-HEAA (1) + HEAPe (2), and (c) CPAc (1) + HEAPe (2). Each panel identifies its measured mole fractions x_1; symbols and curves use a matching symbol–curve pair for each composition.

The fitted parameters and error statistics are listed in Table 8. AARD is 12.76%, 0.92%, and 6.23%, and the largest absolute relative residual is 58.62%, 3.56%, and 23.77% for systems (a), (b), and (c), respectively. The high R^2 for system (a) reflects its broad viscosity range and does not remove the large relative errors at some compositions. With the temperature dependence referred to $T_{ref} = 333.15$ K, the interaction energies $\Delta g_{ij}(T_{ref})$ are well determined, whereas the temperature coefficients Δg_{ij}^1 are smaller than twice their standard errors except Δg_{21}^1 of CPAc + HEAPe. For 2-HEAA + HEAPe, a temperature-independent form with two parameters gives the same AARD (0.93 %). Excluding the estimated viscosity at $x_1 = 0.798$ and 373.15 K (Table 5) changes the fitted coefficients by less than one standard error and the AARD by less than 0.01 percentage

point. The fitted Δg coefficients are empirical correlation parameters, not independently measured mixing energies.

Table 8 Eyring–NRTL parameters and statistics for the interior mixture data; T_{ref} = 333.15 K, uncertainties are standard errors.

	2-HEAA (1) + CPAc (2)	**2-HEAA (1) + HEAPe (2)**	**CPAc (1) + HEAPe (2)**
Δg12(*T*ref) / J·mol⁻¹	20300 ± 6100	8520 ± 230	14200 ± 1200
$\Delta g12^{1}$ / J·mol⁻¹·K⁻¹	30 ± 220	−5.2 ± 7.7	−42 ± 39
Δg21(*T*ref) / J·mol⁻¹	−1660 ± 820	−4001 ± 63	−6040 ± 120
$\Delta g21^{1}$ / J·mol⁻¹·K⁻¹	−30 ± 30	1.1 ± 2.1	−13.0 ± 4.4
R^2	0.9882	0.9997	0.9570
MAE / mPa·s	13.84	5.47	11.85
AARD / %	12.76	0.92	6.23

The Arrhenius equation (12) was fitted to the viscosity data to summarize the apparent temperature dependence over the measured interval:

$$\ln \eta = \ln(\eta_\infty) + \frac{E_\eta}{RT} \tag{12}$$

Here R is the universal gas constant (8.314 J·mol⁻¹·K⁻¹), η_∞ is a formal extrapolation parameter, and E_η is an apparent temperature-slope parameter over the measured interval. In all 32 tabulated pure-component and mixture series, a quadratic function of 1/T improves the corrected AIC by more than 2 relative to the linear Arrhenius relation; the median log-viscosity RMSE decreases by about 92%. Accordingly, the Arrhenius parameters in Tables S5, S7, and S9 summarize the measured interval and should not be interpreted as temperature-independent activation energies or extrapolated beyond it.

3.6 Surface Tension Deviations

Figure 7 shows deviations relative to the mole-fraction-weighted surface tension of the pure components. For 2-HEAA + CPAc (Fig. 7a), the minimum is −5.82 mN·m⁻¹ at x_1 = 0.730 and 303.15 K, well beyond the expanded uncertainty at that point (U = 0.64 mN·m⁻¹, k = 2).

For 2-HEAA + HEAPe (Fig. 7b), all deviation ranges are negative and exceed their expanded uncertainties; the minimum is −8.24 mN·m^{-1} at x_1 = 0.705 and 343.15 K (U = 0.63 mN·m^{-1}).

For CPAc + HEAPe (Fig. 7c), all 54 interior deviations are positive and exceed their pointwise expanded uncertainties, U = 0.61–0.69 mN·m^{-1} (k = 2). The maximum is +11.92 mN·m^{-1} at x_1(CPAc) = 0.775 and 293.15 K; the minimum is +5.01 mN·m^{-1} at x_1(CPAc) = 0.949 and 333.15 K. The mixture surface tensions therefore lie substantially above the mole-fraction-weighted pure-component reference across the measured interior compositions. The Redlich–Kister residual standard deviations for this system are 0.00166–0.00346 mN·m^{-1} across the six temperatures (Table S8, Online Resource 1).

Surface tension is an interfacial property, and the interfacial composition was not measured. The observed Δσ values therefore cannot be assigned uniquely to bulk-volume contraction or to a specific molecular interaction.

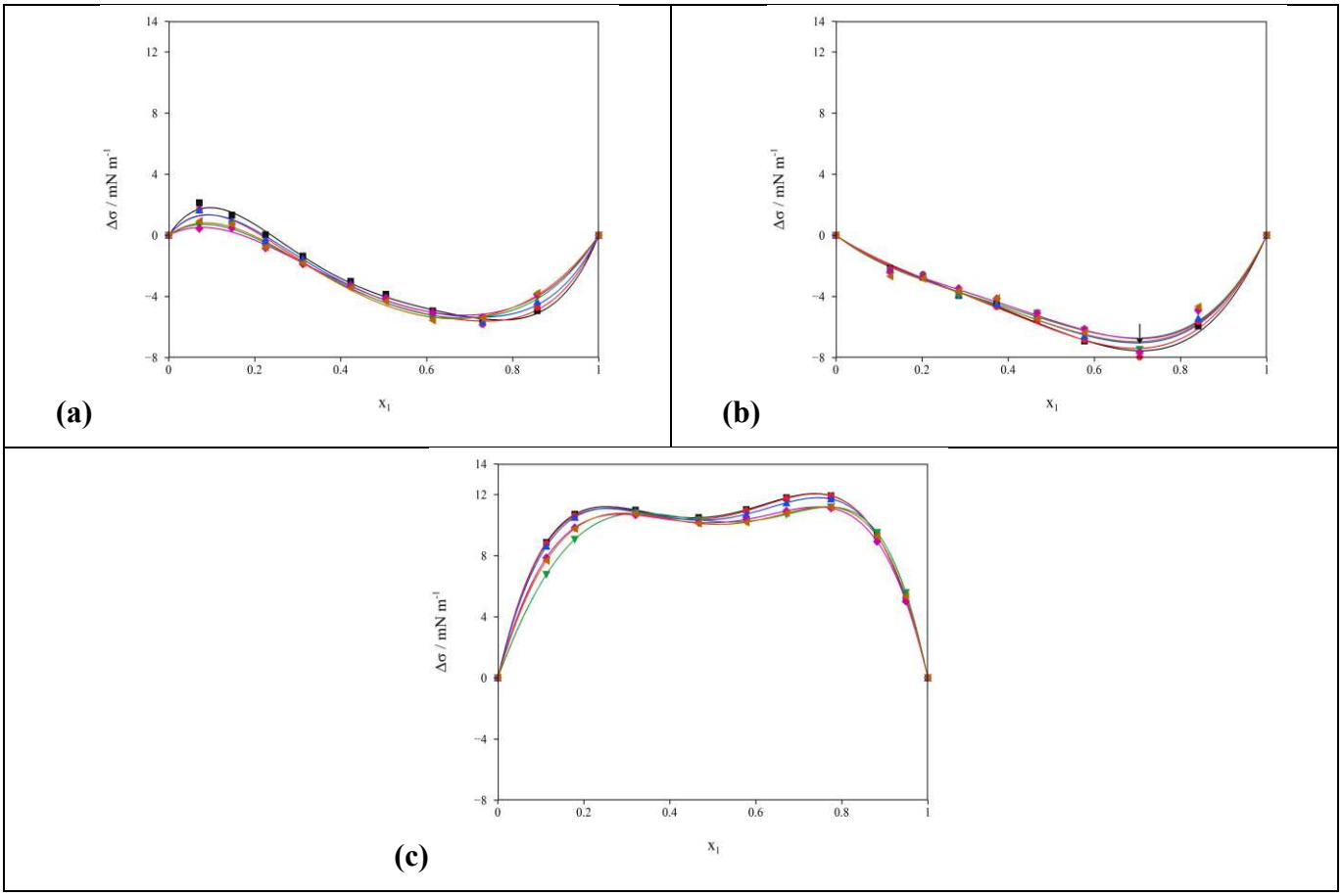


Fig. 7 Surface-tension deviations of (a) 2-HEAA (1) + CPAc (2), (b) 2-HEAA (1) + HEAPe (2), and (c) CPAc (1) + HEAPe (2). Temperatures: (■) 293.15 K, (●) 303.15 K, (▲) 313.15 K, (▼) 323.15 K, (♦) 333.15 K, (◄) 343.15 K. All lines were obtained by polynomial adjustment of Redlich−Kister equation

3.7 Refractive Index Deviations

Figure 8 shows positive refractive-index deviations for most interior compositions. The maxima are 0.0067 for 2-HEAA + CPAc at x_1 = 0.330, 0.0011 for 2-HEAA + HEAPe at x_1 = 0.352, and 0.0174 for CPAc + HEAPe at x_1(CPAc) = 0.887, all at 353.15 K. With U(ΔnD) = 0.0003 (k = 2), every interior deviation of 2-HEAA + CPAc and CPAc + HEAPe exceeds U, whereas only 19 of the 42 interior deviations of 2-HEAA + HEAPe do, all at x_1 = 0.352–0.687. The much larger CPAc + HEAPe deviation is analyzed in Section 3.8.

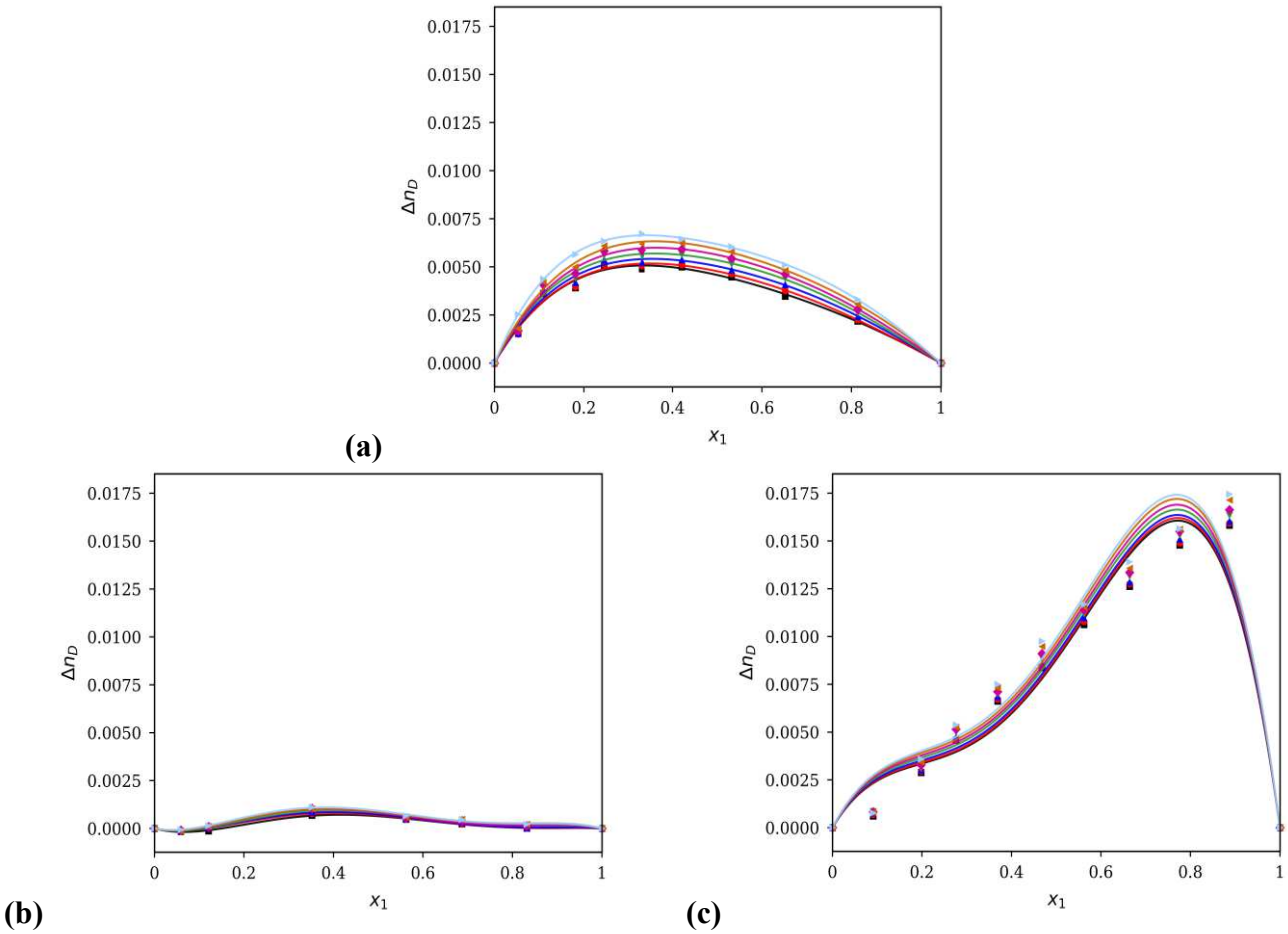


Fig. 8 Influence of temperature on the refractive index deviation of binary mixture: **(a)** 2-HEAA (1) + CPAc (2); **(b)** 2-HEAA (1) + HEAPe (2); **(c)** CPAc (1) + HEAPe (2). Temperatures: (■) 293.15 K, (●) 303.15 K, (▲) 313.15 K, (▼) 323.15 K, (♦) 333.15 K, (◄) 343.15 K, (►) 353.15 K. All lines were obtained from the Redlich-Kister polynomial fit

The Lorentz–Lorenz relation shows that the refractive index depends on both number density and effective polarizability:

$$\frac{n_D^2 - 1}{n_D^2 + 2} = \frac{4\pi}{3}\frac{N_A \alpha_m}{V_m} \tag{13}$$

where α_m is the mean molecular polarizability, N_A is the Avogadro constant, and V $_m$ is the molar volume. Consequently, deviations in n_D can reflect changes in number density and effective polarizability. A negative V^E indicates contraction relative to the ideal-volume reference, but does not identify the cause of an optical deviation.

2-HEAA + HEAPe has the most negative V^E values but Δn_D values that are small (≤ 0.0011) and only partly resolved. The properties therefore do not show a common ranking across the systems. The FTIR spectra were obtained at 298.15 K and cannot establish the mechanism of their trends throughout the wider temperature range.

All Redlich-Kister parameters and standard deviations from the derived properties are presented in the Online Resource 1 (Tables S4, S6, S8 and S10). For CPAc + HEAPe, the three-term Redlich–Kister correlation of Δn_D has s = 0.0018–0.0021, larger than $U(\Delta n_D)$, because Δn_D rises steeply between x_1(CPAc) = 0.887 and 1; it is given only as a smoothing function.

3.8 Refractive Index of CPAc + HEAPe

The CPAc + HEAPe system departs markedly from the other two. Adding 11.3 mol % HEAPe to CPAc raises n_D from 1.4496 to 1.4673 at 293.15 K, and every interior mixture has a refractive index between 1.4653 and 1.4681, close to or slightly above that of pure HEAPe (1.4662). At x_1(CPAc) = 0.887, Δn_D reaches 0.0158 at 293.15 K and 0.0174 at 353.15 K, roughly three times the largest deviation of 2-HEAA + CPAc and more than an order of magnitude larger than that of 2-HEAA + HEAPe (Fig. 8c; Table S11 in Online Resource 1). The deviation decreases almost monotonically toward the HEAPe-rich side, so the optical nonideality is concentrated where small amounts of HEAPe are dispersed in CPAc.

To separate the two contributions in Eq. 13, the molar refraction was evaluated from the measured densities (Table 4):

$$R_m = \frac{M}{\rho}\frac{n_D^2 - 1}{n_D^2 + 2}, \quad R_m^E = R_m - \sum_i x_i R_{m,i} \tag{14}$$

where M is the mole-fraction-weighted molar mass of the mixture and $R_{m,i}$ are the molar refractions of the pure liquids. The two pure components have similar molar refractions, 43.92 $cm^3 \cdot mol^{-1}$ for CPAc and 43.15 $cm^3 \cdot mol^{-1}$ for HEAPe at 293.15 K. If R_m were additive ($R_m^E = 0$), the measured contraction of the mixture volume alone would raise n_D by at most 0.0025 above the linear mole-fraction reference over the whole composition range and temperature interval. The measured Δn_D at x_1(CPAc) = 0.887 is about seven times larger. Reproducing it requires a positive excess molar refraction of +2.6 % at 293.15 K and +3.0 % at 353.15 K, which decreases to +0.1 % at x_1(CPAc) = 0.091. The large Δn_D of CPAc + HEAPe is therefore dominated by an increase in effective polarizability per mole, and only secondarily by tighter packing. For comparison, R_m^E

reaches about +1.7 % in the CPAc-rich region of 2-HEAA + CPAc and about −1.2 % in 2-HEAA + HEAPe, where the volume contraction alone would predict $\Delta n_D \approx 0.007$ but the measured deviations do not exceed about 0.001.

We attribute this behavior to the contrasting molecular architectures of the two liquids. CPAc combines a compact, rigid seven-membered lactam ring with the small acetate anion, a geometry that cannot fill space efficiently and is expected to leave interstitial free volume between the rings. HEAPe contributes a flexible pentanoate anion with a four-carbon alkyl tail and a 2-hydroxyethanaminium cation bearing $–NH_3^+$ and –OH hydrogen-bond donors. When HEAPe is dilute in CPAc, the alkyl tails can occupy the free volume between the lactam rings, while the cation can donate hydrogen bonds to the lactam carbonyl group and to the carboxylate anions. This accommodation is consistent with the volumetric data: at x_1(CPAc) = 0.882, V^E is −0.76 $cm^3 \cdot mol^{-1}$ at 293.15 K and −0.97 $cm^3 \cdot mol^{-1}$ at 353.15 K ($U \approx 0.6$ $cm^3 \cdot mol^{-1}$), so both the contraction and Δn_D increase with temperature at the CPAc-rich end. Hydrogen bonding to the C=O group enhances the polarization of the lactam amide group and the delocalization of its π electrons. In addition, the ordering of chain segments around rigid rings makes the local field anisotropic, which the isotropic Lorentz–Lorenz relation does not account for and which appears as an apparent excess refraction. Both effects raise the effective polarizability above the additive value. The ATR-FTIR spectra of this system are consistent with altered carbonyl and carboxylate environments: features near 1069 and 1526 cm^{-1} move toward 1085 and 1542 cm^{-1}, and the intensities near 1704 and 1255 cm^{-1} change with composition (Section 3.3). The near-constant n_D of all interior mixtures further suggests that about 10 mol % HEAPe is sufficient to restructure the CPAc-rich environment, after which composition has little further effect on the optical response.

Two observations limit the strength of this interpretation. First, an excess molar refraction of about 3 % is larger than the values usually reported for liquid mixtures and larger than those found for the other two systems in this work. Second, Δn_D and R_m^E are referenced to the pure-component values, so their magnitude depends directly on the refractive index of pure CPAc, the lowest of the three liquids. Refractive-index measurements at additional compositions between x_1(CPAc) = 0.887 and 1, together with spectroscopic probes of the lactam carbonyl group, would test the proposed mechanism. The interpretation above is therefore offered as the structural hypothesis most consistent with the present volumetric, optical, and infrared data.

4 Conclusions

Density and dynamic viscosity were measured for the three binary mixtures at 293.15–373.15 K, surface tension at 293.15–343.15 K, and refractive index at 293.15–353.15 K, all at atmospheric pressure. Excess molar volumes are predominantly negative, indicating contraction relative to the ideal-volume reference. Viscosity, surface-tension, and refractive-index deviations depend on composition and temperature and, with the uncertainties evaluated in this work, are resolved at most compositions; V^E of CPAc + HEAPe is resolved only for x_1(CPAc) ≥ 0.671, and all 54 interior $\Delta\sigma$ values of CPAc + HEAPe are positive and exceed their expanded uncertainties. Redlich–Kister correlations describe the reported deviations with system-dependent quality. The Eyring–NRTL model correlates 2-HEAA + HEAPe viscosities closely but has larger relative residuals in the other two systems. The Arrhenius parameters are descriptive over the measured range. For CPAc + HEAPe, the refractive-index deviation of up to 0.017 cannot be explained by volume contraction alone; a Lorentz–Lorenz analysis indicates a positive excess molar refraction of about 3% in the CPAc-rich region, which we attribute to the accommodation of the flexible alkyl chains and hydrogen-bond donors of HEAPe around the rigid lactam rings of CPAc. Apart from this structural hypothesis, the measurements establish nonideal mixing behavior without identifying a unique molecular mechanism.

Supplementary Information

Online Resource 1 contains the ^{1}H NMR spectra; tabulated excess molar volumes and viscosity, surface-tension, and refractive-index deviations; measured-property plots; Redlich–Kister parameters; apparent Arrhenius parameters; Eyring–NRTL residual diagnostics; and pointwise uncertainty calculations.

Statements and Declarations

Funding: This work received financial support from the Conselho Nacional de Desenvolvimento Científico e Tecnológico (CNPq), the Coordenação de Aperfeiçoamento de Pessoal de Nível Superior (CAPES), and the Fundação Cearense de Apoio ao Desenvolvimento Científico e Tecnológico (FUNCAP).

Competing interests: The authors declare no relevant financial or non-financial interests.

Data availability: The experimental and derived data reported in this study are included in this article and in Online Resources 1 and 2.

Author contributions: Francisco M. T. Pereira Filho: Investigation (synthesis of the ionic liquids and the density, viscosity, surface-tension and refractive-index measurements), Formal analysis, Data curation, Visualization, Writing – original draft. Vitor J. Policarpo: Investigation (density, and refractive-index measurements), Data curation, Writing – original draft, Writing – review & editing. Lorena M. Alexandre e Silva and Kirley M. Canuto: Investigation (^{1}H NMR characterization of the ionic liquids), Resources, Writing – review & editing. Filipe X. Feitosa: Conceptualization, Methodology, Supervision, Writing – review & editing. Hosiberto B. de Sant'Ana: Conceptualization, Methodology, Supervision, Project administration, Funding acquisition, Resources, Writing – review & editing. All authors read and approved the final manuscript.

References

[1] Chennuri, B. K.; Gardas, R. L. Measurement and Correlation for the Thermophysical Properties of Hydroxyethyl Ammonium Based Protic Ionic Liquids: Effect of Temperature and Alkyl Chain Length on Anion. Fluid Phase Equilib. 427, 282–290 (2016). https://doi.org/10.1016/j.fluid.2016.07.022

[2] Pires, J.; Timperman, L.; Jacquemin, J.; Balducci, A.; Anouti, M. Density, Conductivity, Viscosity, and Excess Properties of (Pyrrolidinium Nitrate-Based Protic Ionic Liquid + Propylene Carbonate) Binary Mixture. J. Chem. Thermodyn. 59, 10–19 (2013). https://doi.org/10.1016/j.jct.2012.11.020

[3] Anouti, M.; Caillon-Caravanier, M.; Dridi, Y.; Jacquemin, J.; Hardacre, C.; Lemordant, D. Liquid Densities, Heat Capacities, Refractive Index and Excess Quantities for {Protic Ionic Liquids + Water} Binary System. J. Chem. Thermodyn. 41, 799–808 (2009). https://doi.org/10.1016/j.jct.2009.01.011

[4] Khachatrian, A. A.; Shamsutdinova, Z. I.; Rakipov, I. T.; Varfolomeev, M. A.; Solomonov, B. N.; Verevkin, S. P. Hydrogen Bonding of Molecular Solutes in Protic and Aprotic Ionic Liquids. J. Mol. Liq. 271, 815–819 (2018). https://doi.org/10.1016/j.molliq.2018.09.079

[5] Canongia Lopes, J. N. A.; Pádua, A. A. H. Nanostructural Organization in Ionic Liquids. J. Phys. Chem. B 110, 3330–3335 (2006). https://doi.org/10.1021/jp056006y

[6] Triolo, A.; Russina, O.; Bleif, H. J.; Di Cola, E. Nanoscale Segregation in Room Temperature Ionic Liquids. J. Phys. Chem. B 111, 4641–4644 (2007). https://doi.org/10.1021/jp067705t

[7] Wang, Y.; Voth, G. A. Tail Aggregation and Domain Diffusion in Ionic Liquids. J. Phys. Chem. B 110, 18601–18608 (2006). https://doi.org/10.1021/jp063199w

[8] Freire, M. G.; Carvalho, P. J.; Fernandes, A. M.; Marrucho, I. M.; Queimada, A. J.; Coutinho, J. A. P. Surface Tensions of Imidazolium Based Ionic Liquids: Anion, Cation, Temperature and Water Effect. J. Colloid Interface Sci. 314, 621–630 (2007). https://doi.org/10.1016/j.jcis.2007.06.003

[9] Pillai, P.; Kumar, A.; Mandal, A. Mechanistic Studies of Enhanced Oil Recovery by Imidazolium-Based Ionic Liquids as Novel Surfactants. J. Ind. Eng. Chem. 63, 262–274 (2018). https://doi.org/10.1016/j.jiec.2018.02.024

[10] Hallett, J. P.; Welton, T. Room-Temperature Ionic Liquids: Solvents for Synthesis and Catalysis. 2. Chem. Rev. 111, 3508–3576 (2011). https://doi.org/10.1021/cr1003248

[11] Pinheiro, R. S.; Mesquita, F. M. R.; Feitosa, F. X.; Sant'Ana, H. B. de; Santiago-Aguiar, R. S. de. Density, viscosity and excess properties of binary mixtures of protic ionic liquid (2-HDEAF, 2-HDEAA) + water at different temperatures. Braz. J. Chem. Eng. 35, 383–394 (2018). https://doi.org/10.1590/0104-6632.20180352s20160280

[12] Li, Y.; Figueiredo, E. J. P.; Santos, M. J.; Santos, J. B.; Talavera-Prieto, N. M. C.; Carvalho, P. J.; Ferreira, A. G. M.; Mattedi, S. Volumetric and Acoustical Properties of Aqueous Mixtures of N-Methyl-2-Hydroxyethylammonium Butyrate and N-Methyl-2-Hydroxyethylammonium Pentanoate at T = (298.15 to 333.15) K. J. Chem. Thermodyn. 97, 191–205 (2016). https://doi.org/10.1016/j.jct.2016.01.028

[13] Alvarez, V. H.; Mattedi, S.; Martin-Pastor, M.; Aznar, M.; Iglesias, M. Thermophysical Properties of Binary Mixtures of {Ionic Liquid 2-Hydroxy Ethylammonium Acetate + (Water, Methanol, or Ethanol)}. J. Chem. Thermodyn. 43, 997–1010 (2011). https://doi.org/10.1016/j.jct.2011.01.014

[14] Kurnia, K. A.; Taib, M. M.; Abdul Mutalib, M. I.; Murugesan, T. Densities, Refractive Indices and Excess Molar Volumes for Binary Mixtures of Protic Ionic Liquids with Methanol at T=293.15 to 313.15K. J. Mol. Liq. 159, 211–219 (2011). https://doi.org/10.1016/j.molliq.2011.01.005

[15] Duan, Z.; Gu, Y.; Zhang, J.; Zhu, L.; Deng, Y. Protic Pyridinium Ionic Liquids: Synthesis, Acidity Determination and Their Performances for Acid Catalysis. J. Mol. Catal. A Chem. 250, 163–168 (2006). https://doi.org/10.1016/j.molcata.2006.01.035

[16] Kurnia, K. A.; Harris, F.; Wilfred, C. D.; Abdul Mutalib, M. I.; Murugesan, T. Thermodynamic Properties of CO2 Absorption in Hydroxyl Ammonium Ionic Liquids at Pressures of (100-1600) kPa. J. Chem. Thermodyn. 41, 1069–1073 (2009). https://doi.org/10.1016/j.jct.2009.04.003

[17] Yuan, X.; Zhang, S.; Liu, J.; Lu, X. Solubilities of CO2 in Hydroxyl Ammonium Ionic Liquids at Elevated Pressures. Fluid Phase Equilib. 257, 195–200 (2007). https://doi.org/10.1016/j.fluid.2007.01.031

[18] Martinelli, A.; Matic, A.; Jacobsson, P.; Börjesson, L.; Fernicola, A.; Panero, S.; Scrosati, B.; Ohno, H. Physical Properties of Proton Conducting Membranes Based on a Protic Ionic Liquid. J. Phys. Chem. B 111, 12462–12467 (2007). https://doi.org/10.1021/jp0735029

[19] Kachoosangi, R. T.; Musameh, M. M.; Abu-Yousef, I.; Yousef, J. M.; Kanan, S. M.; Xiao, L.; Davies, S. G.; Russell, A.; Compton, R. G. Carbon Nanotube-Ionic Liquid Composite Sensors and Biosensors. Anal. Chem. 81, 435–442 (2009). https://doi.org/10.1021/ac801853r

[20] Greaves, T. L.; Weerawardena, A.; Fong, C.; Krodkiewska, I.; Drummond, C. J. Protic Ionic Liquids: Solvents with Tunable Phase Behavior and Physicochemical Properties. J. Phys. Chem. B 110, 22479–22487 (2006). https://doi.org/10.1021/jp0634048

[21] Yang, J.; Zhang, Q.; Zhu, L.; Zhang, S.; Li, J.; Zhang, X.; Deng, Y. Novel Ionic Liquid Crystals Based on N-Alkylcaprolactam as Cations. Chem. Mater. 19, 2544–2550 (2007). https://doi.org/10.1021/cm062675s

[22] Fendt, S.; Padmanabhan, S.; Blanch, H. W.; Prausnitz, J. M. Viscosities of Acetate or Chloride-Based Ionic Liquids and Some of Their Mixtures with Water or Other Common Solvents. J. Chem. Eng. Data 56, 31–34 (2011). https://doi.org/10.1021/je1007235

[23] Bose, S.; Armstrong, D. W.; Petrich, J. W. Enzyme-Catalyzed Hydrolysis of Cellulose in Ionic Liquids: A Green Approach toward the Production of Biofuels. J. Phys. Chem. B 114, 8221–8227 (2010). https://doi.org/10.1021/jp9120518

[24] Fox, E. T.; Paillard, E.; Borodin, O.; Henderson, W. A. Physicochemical Properties of Binary Ionic Liquid-Aprotic Solvent Electrolyte Mixtures. J. Phys. Chem. C 117, 78–84 (2013). https://doi.org/10.1021/jp3089403

[25] Annat, G.; MacFarlane, D. R.; Forsyth, M. Transport Properties in Ionic Liquids and Ionic Liquid Mixtures: The Challenges of NMR Pulsed Field Gradient Diffusion Measurements. J. Phys. Chem. B 111, 9018–9024 (2007). https://doi.org/10.1021/jp072737h

[26] Bešter-Rogač, M.; Stoppa, A.; Buchner, R. Ion Association of Imidazolium Ionic Liquids in Acetonitrile. J. Phys. Chem. B 118, 1426–1435 (2014). https://doi.org/10.1021/jp412344a

[27] Domańska, U.; Pobudkowska, A.; Rogalski, M. Surface Tension of Binary Mixtures of Imidazolium and Ammonium Based Ionic Liquids with Alcohols, or Water: Cation, Anion Effect. J. Colloid Interface Sci. 322, 342–350 (2008). https://doi.org/10.1016/j.jcis.2008.02.039

[28] Ghasemian, E.; Zobeydi, R. Ionic Liquids Surface Tension Prediction Based on Enthalpy of Vaporization. Fluid Phase Equilib. 358, 40–43 (2013). https://doi.org/10.1016/j.fluid.2013.08.008

[29] Thawarkar, S.; Khupse, N. D.; Shinde, D. R.; Kumar, A. Understanding the Behavior of Mixtures of Protic-Aprotic and Protic-Protic Ionic Liquids: Conductivity, Viscosity, Diffusion Coefficient and Ionicity. J. Mol. Liq. 276, 986–994 (2019). https://doi.org/10.1016/j.molliq.2018.12.024

[30] Anouti, M.; Jacquemin, J.; Porion, P. Transport Properties Investigation of Aqueous Protic Ionic Liquid Solutions through Conductivity, Viscosity, and NMR Self-Diffusion Measurements. J. Phys. Chem. B 116, 4228–4238 (2012). https://doi.org/10.1021/jp3010844

[31] Tokuda, H.; Hayamizu, K.; Ishii, K.; Susan, M. A. B. H.; Watanabe, M. Physicochemical Properties and Structures of Room Temperature Ionic Liquids. 1. Variation of Anionic Species. J. Phys. Chem. B 108, 16593–16600 (2004). https://doi.org/10.1021/jp047480r

[32] Du, Z.; Li, Z.; Guo, S.; Zhang, J.; Zhu, L.; Deng, Y. Investigation of Physicochemical Properties of Lactam-Based Brønsted Acidic Ionic Liquids. J. Phys. Chem. B 109, 19542–19546 (2005). https://doi.org/10.1021/jp0529669

[33] Álvarez, V. H. Termodinâmica e Aplicações de Líquidos Iônicos. PhD Thesis, Universidade Estadual de Campinas (2010).

[34] Bessa, A. M. M.; Venerando, M. S. C.; Feitosa, F. X.; Alexandre e Silva, L. M.; Fernandes, F. A. N.; de Santiago-Aguiar, R. S.; de Sant'Ana, H. B. Low Viscosity Lactam-Based Ionic Liquids with Carboxylate Anions: Synthesis, Characterization, Thermophysical Properties and Mutual Miscibility of Ionic Liquid with Alcohol, Water, and Hydrocarbons. J. Mol. Liq. 313, 113586 (2020). https://doi.org/10.1016/j.molliq.2020.113586

[35] Pereira Filho, F. M. T.; de Medeiros, L. H. G.; Alexandre e Silva, L. M.; Canuto, K. M.; Feitosa, F. X.; de Sant'Ana, H. B. Density for M−2−HEAA + 2-HEAA and HEAPe + 2-HEAA Binary Mixtures and Pure Compounds at High Pressure. J. Chem. Thermodyn. 203, 107429 (2025). https://doi.org/10.1016/j.jct.2024.107429

[36] de Medeiros, L. H. G.; da Costa, M. F. L.; Bazile, J.-P.; Feitosa, F. X.; de Sant'Ana, H. B.; Daridon, J.-L. A Combined Experimental and PC-SAFT Modeling Investigation on the High-Pressure Density of Ionic Liquids with CO_2. J. Chem. Eng. Data 71, 1630–1640 (2026). https://doi.org/10.1021/acs.jced.5c00790

[37] Klomfar, J.; Součková, M.; Pátek, J. Surface Tension Measurements with Validated Accuracy for Four 1-Alkyl-3-Methylimidazolium Based Ionic Liquids. J. Chem. Thermodyn. 42, 323–329 (2010). https://doi.org/10.1016/j.jct.2009.09.007

[38] Harkins, W. D.; Jordan, H. F. A Method for the Determination of Surface and Interfacial Tension from the Maximum Pull on a Ring. J. Am. Chem. Soc. 52, 1751–1772 (1930). https://doi.org/10.1021/ja01368a004

[39] Buarque, F. S.; Camêlo, L. C. A.; Soares, C. M. F.; Mattedi, S.; Ferreira, A. F. B.; Feitosa, F. X.; Souza, R. L.; de Sant'Ana, H. B.; Lima, Á. S. Binary Mixture of Double Protic Ionic Liquid: Density, Viscosity, Refractive Index, Surface Tension, and Derivative Properties. J. Chem. Eng. Data 66, 4309–4325 (2021). https://doi.org/10.1021/acs.jced.1c00429

[40] Wang, Y. G.; Chen, D. X.; Ouyang, X. K. Viscosity Calculations for Ionic Liquid-Cosolvent Mixtures Based on Eyring's Absolute Rate Theory and Activity Coefficient Models. J. Chem. Eng. Data 55, 4878–4884 (2010). https://doi.org/10.1021/je100487m

[41] Dias, R. M.; Sosa, F. H. B.; da Costa, M. C. Dissolution of Lignocellulosic Biopolymers in Ethanolamine-Based Protic Ionic Liquids. Polym. Bull. 77, 3637–3656 (2020). https://doi.org/10.1007/s00289-019-02929-2

[42] Pinkert, A.; Ang, K. L.; Marsh, K. N.; Pang, S. Density, Viscosity and Electrical Conductivity of Protic Alkanolammonium Ionic Liquids. Phys. Chem. Chem. Phys. 13, 5136–5143 (2011). https://doi.org/10.1039/c0cp02222e

[43] Iglesias, M.; Gonzalez-Olmos, R.; Cota, I.; Medina, F. Brønsted Ionic Liquids: Study of Physico-Chemical Properties and Catalytic Activity in Aldol Condensations. Chem. Eng. J. 162, 802–808 (2010). https://doi.org/10.1016/j.cej.2010.06.008

[44] Pinto, R. R.; Santos, D.; Mattedi, S.; Aznar, M. Density, refractive index, apparent volumes and excess molar volumes of four protic ionic liquids + water at T = 298.15 and 323.15 K. Braz. J. Chem. Eng. 32, 671–682 (2015). https://doi.org/10.1590/0104-6632.20150323s00003444

[45] Chhotaray, P. K.; Jella, S.; Gardas, R. L. Physicochemical Properties of Low Viscous Lactam Based Ionic Liquids. J. Chem. Thermodyn. 74, 255–262 (2014). https://doi.org/10.1016/j.jct.2014.02.009

[46] Jiang, B.; Yang, H.; Zhang, L.; Zhang, R.; Sun, Y.; Huang, Y. Efficient Oxidative Desulfurization of Diesel Fuel Using Amide-Based Ionic Liquids. Chem. Eng. J. 283, 89–96 (2016). https://doi.org/10.1016/j.cej.2015.07.070

[47] Karlapudi, S.; Prasad, C.; Olasunkanmi, L. O.; Singh, S.; Bahadur, I.; Siva Kumar, K.; Ebenso, E. E. Hydrogen Bonding Interactions of m-Chlorotoluene with 1-Alkanol Analyzed by Thermodynamic, Fourier Transform Infrared Spectroscopy, Density Functional Theory, and Natural Bond Orbital. ACS Omega 3, 4679–4687 (2018). https://doi.org/10.1021/acsomega.7b01834

[48] Królikowska, M.; Zawadzki, M.; Domańska, U.; Ramjugernath, D.; Naidoo, P. The Influence of Temperature and Composition on the Density, Viscosity and Excess Properties of Aqueous Mixtures of Carboxylic-Based Ionic Liquids. J. Chem. Thermodyn. 109, 71–81 (2017). https://doi.org/10.1016/j.jct.2016.10.034

[49] Bing, X.; Meng, X.; Li, A.; Zhang, L.; Gao, J.; Xu, D.; Wang, Y. Extraction and Mechanism Exploration for Separating Cresols from Coal Tar by Ionic Liquid Ethanolamine Lactate. J. Mol. Liq. 305, 112845 (2020). https://doi.org/10.1016/j.molliq.2020.112845

[50] Zhang, Q.; Liu, D.; Li, Q.; Zhang, X.; Wei, Y. Density, Electrical Conductivity, Dynamic Viscosity, Excess Properties, and Molecular Interactions of Ionic Liquid 1-Cyanopropyl-3-Methylimidazolium Tetrafluoroborate and Binary System with Acetonitrile. J. Chem. Eng. Data 63, 1256–1265 (2018). https://doi.org/10.1021/acs.jced.7b00898

[51] Guevara-Carrion, G.; Hasse, H.; Vrabec, J. Thermodynamic Properties for Applications in Chemical Industry via Classical Force Fields. Top. Curr. Chem. 307, 201–249 (2012). https://doi.org/10.1007/128_2011_164

Supplementary Files

This is a list of supplementary files associated with this preprint. Click to download.

- OnlineResource1IJT.docx